Hybrid Excitation Method for Higher Pole Number Grid-Tie Synchronous Generators

Dillan K. Ockhuis, *Student Member, IEEE*, Maarten J. Kamper, *Senior Member, IEEE* and Andrew T. Loubser
Department of Electrical and Electronic Engineering, Stellenbosch University, South Africa
d.ockhuis09@gmail.com; kamper@sun.ac.za; atloubser@sun.ac.za

***Abstract*—In this paper, a hybrid excitation method is proposed and evaluated for classical rotor-excited higher pole number synchronous machines. The hybrid excitation is obtained by means of an integrated parallel hybrid-excited rotor using permanent magnets and field windings. Synchronous machines with both overlap and non-overlap stator windings are considered. The investigation is done by means of frozen permeability finite element analysis. It is explained that the method is applicable for synchronous machines with pole numbers of eight and higher. Detailed information is given of the variable-flux and number-of-parallel-circuit possibilities for a series of higher pole number synchronous machines. The results presented of a 15 kW, 48-pole synchronous machine prove that the method is excellently suited for grid-tie synchronous generators.**

***Index Terms*—hybrid excitation, synchronous machine, permanent magnet, overlap winding, non-overlap winding, rotor excitation.**

I. Introduction

The use of permanent magnet (PM) material in electric synchronous machines has the important advantages of increased power density and efficiency. One disadvantage of using permanent magnets is that the PM-generated flux is fixed in the machine and hence flux adjustment cannot be done. Flux adjustment is important in adjustable speed applications such as electric vehicles [1]. Yet in most of the adjustable speed applications with interior PM-synchronous motors and solid-state converters, a wide speed range can be obtained without adjusting the generated PM flux in the motor. However, in power synchronous generator applications where the generator must operate at a fixed frequency and at a reasonably fixed voltage, generated flux adjustment in the machine is an absolute necessity. Examples of such applications are auxiliary power supplies, such as for ships, and grid-tie energy generation, such as hydroelectric power generation [2]. The focus of the paper is on the latter applications using PM generators with excited flux adjustment.

In the last three decades, many proposals have been made to obtain excited flux adjustment in PM generators by means of hybrid excitation, that is through the use of both PM and field-winding excitations [1] - [11]. The proposed methods can be divided into two groups, namely series hybrid-excitation where the PM and field-winding work magnetically in series, or parallel hybrid excitation, where the PM and field-winding work magnetically in parallel. The proposed PM generators can also be divided into three groups, namely (i) hybrid excitation on the rotor of a conventional synchronous machine, (ii) hybrid excitation on the stator of a dual-spoke synchronous machine with a passive rotor (flux-switching machine) and (iii) hybrid excitation which is divided between the rotor and the stator of the synchronous machine using complex 3D field-circuit structures. An overview of the hybrid excitation technology is given in [12]. The focus of the paper is on the first group of hybrid generators, where the hybrid excitation is on the rotor. With this hybrid-excited generator, the concept is still simple and standard, and good quality sinusoidal voltages are generated.

Of the rotor hybrid excitation synchronous generators, series hybrid excitation is most commonly used [1], [7], [9], [10]. The disadvantage of series hybrid excitation is the relatively large field-winding MMF needed due to the relatively large effective air gap; therefore, the magnet thickness is relatively thin in these designs, but this in turn results in low open-circuit, zero field-current generated voltage [10]. A classical parallel hybrid-rotor excitation method referred to by many is found in [5]. The other parallel hybrid excitation methods used are where the magnets are placed in the slot openings of the field winding, with the magnets tangentially magnetized [8], [10], [11]. This method, however, is used more to enhance the ability of the ordinary field-winding excited generator (thus not a PM generator), and thus these generators are also referred to as PM-assisted synchronous generators. A last parallel hybrid method proposed is found in [2], where the PM excitation and field-winding excitation are done separately by means of two separate rotors mounted in tandem on the rotor shaft. This method is probably the best parallel hybrid excitation method; however, at the expense that part of the stator's axial length is not used actively; the rotor construction is also somewhat complex, especially in the case of a generator with an external rotating rotor.

With the requirements of designing a grid-connected, hybrid-excited rotor-PM synchronous generator that should (i) generate close to rated voltage with zero field excitation current and (ii) obtain a reasonably large variation in the generated flux, the series-hybrid excitation method is not suitable. With the disadvantages of the parallel/separate hybrid rotor excitation method of [2], this paper again focuses on the classic parallel hybrid-excitation method of [5]. The disadvantages of this method are pointed out in the paper and an improved parallel hybrid excitation method is proposed. The main focus of the paper is on synchronous generators with higher pole numbers using non-overlap stator windings.

This work was financially supported by the Centre for Renewable and Sustainable Energy Studies at Stellenbosch University, South Africa.

978-1-7281-5826-6/20/$31.00 ©2020 IEEE

II. Hybrid Excitation Method of [5]

The most cited paper on the topic of hybrid excitation is the paper of [5]. Yet it is interesting that no further attention has been paid in the published research to this parallel hybrid excitation method. The method is also not investigated in any detail regarding the effect of magnetic saturation. In this section, we investigate this proposed method further.

The cross-section of the hybrid-excited rotor synchronous machine proposed by [5] is shown in Fig. 1(a). The generator has 36 slots and six poles, of which four poles are PM poles and two poles are field-winding poles. It is clear in this case that the maximum number of parallel circuits of the stator is two, since a series-connected phase group must span across two PM poles and one field-winding pole. The latter is important because, if the generator was just an ordinary six-pole PM generator, then up to six parallel circuits could be used. In this regard it already points out the disadvantage of this method of parallel hybrid excitation, an aspect that is further considered later in the paper.

When the effect of magnetic saturation in the magnetic equivalent circuit of the machine in Fig. 1(a) is taken into account, it is clear that the large stator yoke reluctances that magnetically link the two field-winding poles disturb the parallel, independent action between the magnet and field excitations. This means that a much larger change in the field MMF is needed to get a certain change in flux linkage and induced voltage, which impairs the efficiency of the generator.

Finally, a comment must be made about the use of negative field current in the machine in Fig. 1(a). This is proposed by [5] to get a wider variation in flux. With negative field current, the field winding poles swap which in effect changes the rotor to a two-pole rotor, as indicated by the north-south indications on the rotor in Fig. 1(a). A two-pole rotor per se is not a problem, because there is still a six-pole stator winding. However, with two-pole flux, the small six-pole designed stator yokes will undergo severe saturation unless they are designed to be large, which increases the mass and is uneconomical. Hence, in this paper the use of negative field current is not followed.

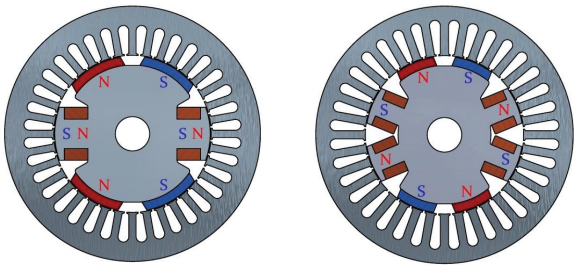

(a) (b)

Fig. 1. (a) Six-pole hybrid rotor-excited synchronous machine [5] and (b) eight-pole synchronous machine with proposed parallel hybrid-excited rotor.

III. Proposed Hybrid Method

In order to minimise the problem of the effect of magnetic saturation in the machine of Fig. 1(a) and to obtain an improved parallel hybrid excitation, the following requirements are set with respect to the layout of the hybrid rotor of integral, overlap stator-winding synchronous machines:

(i) A minimum of two field-winding poles (p_f) must always be placed adjacently on the rotor. This is to shorten the stator yoke part that magnetically links the two field winding poles. To avoid unbalanced magnetic pull in the machine, a further minimum of two adjacent field-winding poles must be located on the opposite side of the rotor, thus displaced 180° apart mechanically. This means that there should be a minimum of four field-winding poles on the rotor.

(ii) Similarly, a minimum of two PM poles (p_m) must always be placed adjacently on the rotor and therefore there also should be at least two additional, adjacent PM poles on the opposite side of the rotor. This requires that there should also be a total of at least four PM poles.

With these requirements, it means that the generator must have atleast eight poles or more. Therefore, for an eight-pole generator (p = 8), only one layout will be possible, namely four field poles (p_f = 4) and four PM poles (p_m = 4), as shown in Fig. 1(b). One can see in Fig. 1(b) how two field-winding poles are together and how two magnet poles are together. For a 12-pole generator, there will be two layout options, namely six field poles and six PM poles, or four field poles and eight PM poles. In general, for overlap stator-winding machines, we thus have the hybrid pole conditions as given by (1). Note in (1) that $p_m \geqslant p_f$ because the machine is mainly a PM machine, with only some additional flux variability by means of the field winding. The maximum number of parallel circuits, $a_{\max}$, can be determined for integral overlap stator windings by (2).

$$\begin{aligned} p &= p_f + p_m \geqslant 8 \\ p_f &\geqslant 4; \quad p_f = \text{even} \\ p_m &\geqslant 4; \quad p_m = \text{even} \\ p_m &\geqslant p_f \end{aligned} \tag{1}$$

$$\begin{aligned} a_{\max} &= 2n_{\max} \quad \text{with} \\ n_{\max} &= \begin{bmatrix} n = 1, 2, 3, ... \\ \frac{p_f}{2n} = 2, 3, 5, 7, ... \\ n \rightarrow \text{maximised} \end{bmatrix} \end{aligned} \tag{2}$$

For non-overlap stator-windings, the above-mentioned saturation problem of the machine in Fig. 1(a) is, for all practical reasons, not an issue. The reason for this is that almost all non-overlap windings have two or more north-south adjacent poles in a series-connected winding section. Thus, for non-overlap winding machines, we need to consider only winding-pole sections (W_s) instead of number of poles. Hence, we divide the machine into a number of wound-pole sections (W_f) and magnet-pole sections (W_m). For balanced magnetic pull, the rotor must have at least two wound-pole sections on opposite sides of the rotor and two magnet-pole sections on opposite sides of the rotor. The conditions required for non-overlap

winding machines are given by (3), with N_s the number of stator slots. Note we consider in (3) only three-phase, double-layer, side-by-side stator windings. Similar as in (1), we have $W_m \geq W_f$ because the machine is a PM machine with only some variable field flux excitation.

$$\begin{aligned} &W_s = \gcd(p, N_s) \quad \text{and} \quad u = N_s/(3W_s) = 2, 3, 4, ... \\ &W_s = W_f + W_m \geq 4 \\ &W_f \geq 2; W_m \geq 2; W_m \geq W_f; W_m/W_f = \text{integer} \\ &a_{\max} = W_f \\ &p_f = p\frac{W_f}{W_s}; \quad p_m = p\frac{W_m}{W_s}. \end{aligned} \tag{3}$$

In Table I, a 48-pole machine is considered as an example of the hybrid rotor possibilities of a synchronous machine with an integral overlap stator winding. In Table II we consider the hybrid rotor possibilities of two different pole-number synchronous generators with good winding-factor, non-overlap stator windings. From the figures in both tables it is evident that the number of parallel circuits is limited, and so also the number of possible pole-slot combinations of non-overlap winding machines. However, in general, the higher the pole number of the generator, the more the hybrid rotor pole and winding layout possibilities become.

TABLE I
HYBRID ROTOR EXCITATION POSSIBILITIES OF 48-POLE INTEGRAL OVERLAP WINDING SYNCHRONOUS MACHINES.

$p = 48$								
p_f	10	12	14	16	18	20	22	24
p_m	38	36	34	32	30	28	26	24
$a_{\max}$	2	6	2	8	2	4	2	12
r	5/9	1/3	7/17	1/2	9/15	5/7	11/13	1
$\pm\Delta V$ (%)	11.6	14.3	17.1	20	23.1	26.3	29.7	33.3

TABLE II
HYBRID ROTOR EXCITATION POSSIBILITIES OF 40- AND 48-POLE NON-OVERLAP WINDING SYNCHRONOUS MACHINES.

p = 40								
N_s	W_s	W_f	W_m	p_f	p_m	$a_{\max}$	r	$\pm\triangle V$ (%)
36	4	2	2	20	20	2	1	33.3
48	8	2	6	10	30	2	1/3	14.3
		4	4	20	20	4	1	33.3
p = 48								
54	6	2	4	16	32	2	1/2	20
		3	3	24	24	3	1	33.3

IV. Variable Voltage Method

As explained in the introduction, with generators that operate at fixed frequencies and at reasonable fixed voltages, such as in the case of direct grid connection, the open-circuit, zero field-current induced-voltage of the generator cannot be far below the rated voltage of the machine. Furthermore, it makes great sense to use the availability of the wound-field rotor excitation to help generate the rated power and rated voltage.

From the above, we propose that the rated voltage of the generator must be induced at open-circuit with half the rated field current. The lowest open-circuit induced voltage is then obtained with zero field current and the highest induced voltage with rated field current. This method of voltage variation with field current variation is explained in Fig. 2. The degree of voltage variation depends on the ratio r of the wound-field poles to the PM poles or, for the non-overlap winding machines, the ratio of the wound-field pole sections to the magnet pole sections, hence expressed as

$$r = \frac{p_f}{p_m} = \frac{W_f}{W_m}. \tag{4}$$

With this, and assuming a linear voltage variation as in Fig. 2, the per unit open-circuit voltage of the generator can be expressed by

$$V = \left(\frac{2r}{2+r}\right) I_{f(\text{pu})} + \frac{2}{2+r} \quad (\text{pu}) \tag{5}$$

and the percentage voltage variation by

$$\pm\Delta V = \pm\frac{r}{2+r} \times 100\%. \tag{6}$$

In general, a minimum of $\pm 10\%$ voltage variation is required for grid-connected generators, which requires the ratio r to be $r \geq 0.23$. With the maximum ratio possible of r = 1, the maximum voltage variation is theoretically $\pm 33.3\%$, which can be considered as relatively large. Hence the ratio between the wound-field and magnet poles/sections in this method is always in the range of $0.23 \leq r \leq 1$. In Tables I and II the ratios and percentage voltage variations of the machines under consideration are given. There are examples of small percentage (11.6%) and large percentage (33.3%) voltage variations. It is clear that one can select an option according to the required voltage variation. Finally, the linear voltage variation in Fig. 2 obviously depends on the degree of saturation.

V. Non-Overlap Winding Generator

In this section we investigate a particular case by means of finite element (FE) analysis. The machine we consider is the 48-pole, 54-slot, non-overlap winding machine highlighted in Table II. The machine has two wound-field poles and four magnet-pole sections, with a theoretical $\pm 20\%$ voltage variation. The cross-section of the FE model of this machine is shown in Fig. 3. It has six winding sections, where each section

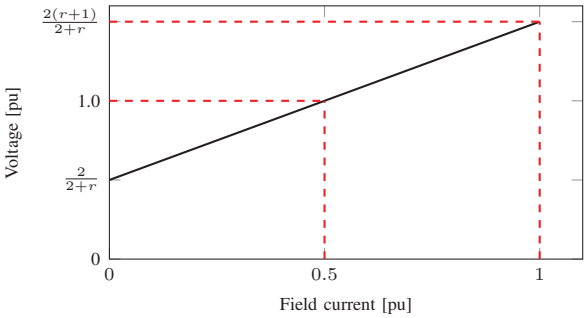

Fig. 2. Method of per unit voltage variation versus per unit field current variation.

has eight poles. The detailed specifications of the generator are given in Table III.

It can be seen from the generator in Fig. 3 that large open slots are used for the stator and wound-rotor part. The reason for this is the use of pre-wound coils that are inserted into the slots. The large open slots also reduce the stator slot leakage reactance. The rotor field winding has eight side-by-side DC-winding coils. These coils are connected in series to ensure that the net induced field-winding voltages, caused by the travelling stator-MMF-harmonic fluxes, is zero.

A stator winding section of the generator consists of eight poles and nine slots. The eight-nine pole-slot combination generates the MMF harmonics as shown in Fig. 4. The relatively large sub- and higher-order harmonics are classical for these non-overlap windings. These MMF harmonics generate a large amount of harmonic leakage flux in the machine, which causes the harmonic leakage coefficient τ_d to be large, as indicated in Table III. This, in turn, increases the net synchronous reactance of the machine, an aspect that is important for grid connection and that is considered further in Section VII. To reduce the core losses due to the harmonic-generated fluxes, the magnets are segmented and the rotor core is laminated. The core losses in the wound-rotor part of the rotor in Fig. 3, however, may be severe due to the much larger harmonic fluxes in the rotor because of the small air gap in that part of the machine. The core losses are evaluated in Section VII.

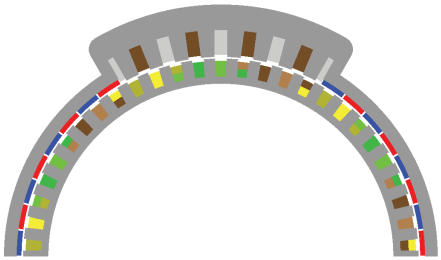

Fig. 3. Finite element cross-section model of a 15 kW, 48-pole hybrid-excited generator.

TABLE III
SPECIFICATIONS OF THE HYBRID-EXCITED GENERATOR

Rated power	15 kW
Rated voltage	400 V
Rated stator current	21 A
Rated frequency	50 Hz
Rated speed	125 r/min
Number of poles	48
Number of stator slots and stator coils	54
Number of parallel stator circuits	2
Open circuit voltage variation	$\pm$ 20%
Stator working harmonic winding factor (k_{w4})	0.945
Harmonic leakage flux coefficient τ_d	1.175
Number of magnet poles	32
Number of wound-field poles	16
Number of rotor field slots and field coils	16
Stator inner diameter	530 mm
PM rotor outer diameter	655 mm
Wound rotor outer diameter	740 mm
Axial stack length	114 mm
Airgap length	1.8 mm
RMS stator current density	6.0 A/mm^2
Rated (maximum) field current density	6.0 A/mm^2

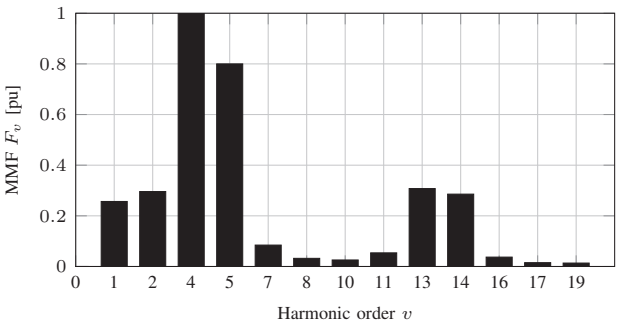

Fig. 4. Per unit stator MMF harmonics of the generator. The working harmonic is v = 4.

The flux density field line plots of this machine without and with wound-field excitation as illustrated in Fig. 5 clearly show the action of hybrid rotor field excitation. FE analysis is used to determine the d-axis flux linkages to calculate the induced voltage versus field current of the machine. This result is shown in Fig. 6, where a $\pm$20% voltage variation is obtained for the rated 400 V machine in Fig. 3.

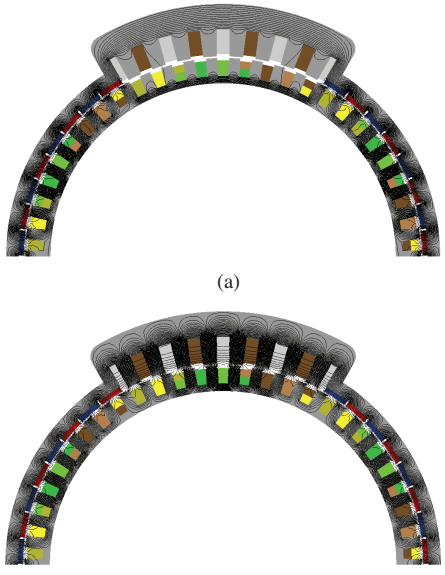

Fig. 5. Flux density field line plots with (a) zero and (b) rated wound-field excitation.

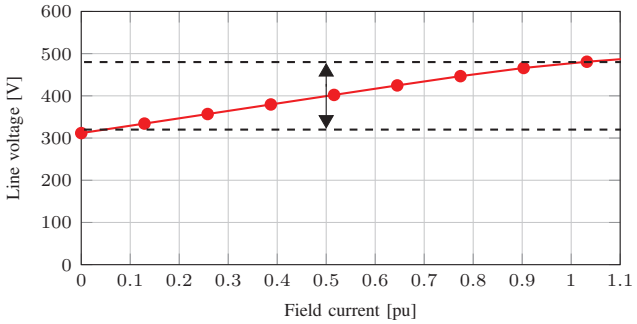

Fig. 6. Open-circuit FE calculated line voltage versus per unit field current of the machine in Fig. 3 where 400 V is the rated voltage.

VI. FE Modelling and Performance Calculation

In this section we briefly consider the FE modelling of the inductances of the generator, and a solution method is provided for performance estimation at specific power and reactive power operating points.

A. Frozen permeability FE inductance modelling

In FE modelling, we make use of the frozen permeability (FP) technique to investigate the exact flux contribution of the wound-field poles and magnet poles to the total flux linkage. The latter is particularly important under load conditions. Furthermore, with the hybrid-excited rotor, it is very important to understand the effective self- and mutual inductances of the machine. Consequently, we express, in steady state, the dq flux linkages in the generator reference frame (positive current flowing out of the machine) to take the effects of saturation and cross-magnetisation into account, as

$$\lambda_d = -L_d I_d - M_{dq} I_q + L_{df} I_f + \lambda_{dm} \tag{7}$$

$$\lambda_q = -L_q I_q - M_{qd} I_d + L_{qf} I_f + \lambda_{qm}. \tag{8}$$

The inductances of (7) and (8) are all accurately determined by means of the FE-FP technique. Note from (8) that we take the q-axis flux linkages due to the field-winding and the magnets into account. In this way, we evaluate the effects of the integrated wound-field poles on the performance of the grid-connected hybrid-excited synchronous machine.

B. Performance calculation

To determine the performance of the generator in the steady state, we use the dq voltage equations with generator reference, as

$$V_d = \sqrt{\frac{2}{3}} V_L \sin(\Delta) = -R_s I_d - \omega \lambda_q \tag{9}$$

$$V_q = \sqrt{\frac{2}{3}} V_L \cos(\Delta) = -R_s I_q + \omega \lambda_d, \tag{10}$$

where Δ is the classical power angle between the q-axis and the voltage phasor, which is positive for generator mode. The power and reactive power at the grid are calculated by

$$P = \sqrt{\frac{3}{2}} (V_d I_d + V_q I_q) \tag{11}$$

$$Q = \sqrt{\frac{3}{2}} (V_q I_d - V_d I_q). \tag{12}$$

The efficiency is calculated as

$$\eta = \frac{P}{\tau \omega_m + P_{core}}, \tag{13}$$

where τ is the generator developed torque, which is given by

$$\tau = \frac{3}{2} p (\lambda_d I_q - \lambda_q I_d), \tag{14}$$

and P_{core} in (13) is the stator and rotor core losses calculated from rotor position-stepped FE analysis. In (13) we ignore the eddy current losses in the stator conductors and the winding and friction losses of the generator.

C. Performance solution at P^* and Q^* operating points

The performance of the generator needs to be determined at the desired power P^* and reactive power Q^* operating points. We see from (7), (8), (9) and (10) that there are four unknown variables for the grid-connected generator, namely I_d, I_q, I_f and Δ. With the FP-technique, the inductances and PM flux linkages of (7) and (8) can be determined by using initial dq currents. If Δ and I_f are given, then we can solve for I_d and I_q in an iterative convergent way, as expressed by (15). With the dq voltages and currents known, P and Q can be solved from (11) and (12), as shown in (15).

$$\text{Given} \rightarrow \begin{bmatrix} \Delta \\ I_f \\ V_L \end{bmatrix} \rightarrow \boxed{\begin{array}{c}\text{Iteratively solve with FP-} \\ \text{-method the } dq \text{ currents} \\ \text{from (7), (8), (9), (10)}\end{array}} \Rightarrow \begin{bmatrix} I_d \\ I_q \end{bmatrix} \Rightarrow \begin{bmatrix} P \\ Q \end{bmatrix} \tag{15}$$

An estimated value for Δ is first determined to come close to the desired P^* and Q^* power operating points. For this we approximate the machine model by ignoring saliency and cross-coupling effects and ignoring the stator resistance. From this it can be shown that Δ can be determined approximately by

$$\Delta \approx \tan^{-1} \left[\frac{P^* X_s}{Q^* X_s + V_L^2} \right]. \tag{16}$$

In (16), all the parameters are given in per unit. We estimate that the per unit value of the synchronous reactance X_s in (16) for the machine of Fig. 3 is about X_s = 0.5 pu [13]. Since P and Q are smooth functions of Δ and I_f, (15) is used to determine interpolating polynomial functions that are used to analytically quickly calculate the performance of the generator over its whole power operating region. A second-degree interpolating polynomial requires only three data points per curve fitting. Hence, Δ and I_f are varied from minimum to maximum with three data values, $\Delta_{i=1,2,3}$ and $I_{fj=1,2,3}$, as

$$\mathbf{\Delta} = \begin{bmatrix} \Delta_1 = \Delta_{\min} \\ \Delta_2 = \frac{1}{2}(\Delta_{\min} + \Delta_{\max}) \\ \Delta_3 = \Delta_{\max} \end{bmatrix} \text{(a)}; \mathbf{I_f} = \begin{bmatrix} I_{f1} = 0.0 \text{ pu} \\ I_{f2} = 0.5 \text{ pu} \\ I_{f3} = 1.0 \text{ pu} \end{bmatrix} \text{(b)}, \tag{17}$$

where $\Delta_{\min}$ and $\Delta_{\max}$ are estimated from (16) for the whole power operating region of the generator. Using this as input to (15), the power data of the generator can be determined as

$$\mathbf{P_{ij}} = \begin{bmatrix} P_{11} & P_{12} & P_{13} \\ P_{21} & P_{22} & P_{23} \\ P_{31} & P_{32} & P_{33} \end{bmatrix} \text{(a)}; \mathbf{Q_{ij}} = \begin{bmatrix} Q_{11} & Q_{12} & Q_{13} \\ Q_{21} & Q_{22} & Q_{23} \\ Q_{31} & Q_{32} & Q_{33} \end{bmatrix} \text{(b)}. \tag{18}$$

With second-degree interpolating polynomials, analytical functions can be obtained from the data of (17) and (18) as

$$\Delta_j = f(P, I_f = I_{fj}) \tag{19}$$

$$Q_j = f(\Delta, I_f = I_{fj}) \tag{20}$$

for j = 1, 2, 3. From (19) we generate the data for Δ that satisfies $P = P^*$, that is

$$\Delta_{xj} = f(P = P^*, I_f = I_{fj}) \rightarrow \mathbf{\Delta_{xj}}_{\{P=P^*\}} = \begin{bmatrix} \Delta_{x1} \\ \Delta_{x2} \\ \Delta_{x3} \end{bmatrix}. \tag{21}$$

Using the Δ_{xj} data of (21) as input in (20), we generate the data for $\mathbf{Q}$ that satisfies $P = P^*$ as

$$Q_{xj} = f(\Delta = \Delta_{xj}, I_f = I_{fj}) \rightarrow \mathbf{Q_{xj}}_{\{P=P^*\}} = \begin{bmatrix} Q_{x1} \\ Q_{x2} \\ Q_{x3} \end{bmatrix}. \quad (22)$$

Again, second-degree interpolating polynomial functions can be obtained from the data of (21) and (22), as well as from the data of (17b) and (22), as

$$\Delta = f(Q, P = P^*) \quad (23)$$

$$I_f = f(Q, P = P^*) \quad (24)$$

From the above, note that (17) to (20) need only to be done once, hence Δ_x and I_{fx} can then be determined fast for different P^* and Q^* desired power values.

VII. Performance Evaluation

In this section, the performance of the hybrid-excited generator in Fig. 3 is evaluated by first comparing its performance to that of the PM-excited generator. Secondly the performance is evaluated at various operating conditions according to grid-code requirements. The different performance parameters considered are the torque ripple, core losses, efficiency, reactive power and per unit synchronous reactance. Regarding the latter, the following per unit impedance and voltage parameters are considered in the performance evaluation:

$$V_{d(\text{pu})} = -R_s I_d + X_q I_q + \{X_{qd}\} I_d - E_{qmf} \quad (25)$$

$$V_{q(\text{pu})} = -R_s I_q + X_d I_d + \{X_{dq}\} I_q - E_{dmf}, \quad (26)$$

where

$$\begin{aligned} E_{dmf} &= \omega(L_{df} I_{df} + \lambda_{dm}) \\ E_{qmf} &= \omega(L_{qf} I_{qf} + \lambda_{qm}). \end{aligned} \quad (27)$$

The parameters in curly brackets in (25) and (26) are ignored in classical dq analysis.

A. Comparison between PM and hybrid excitation

In the performance comparison between the PM- and hybrid-excited generators, we focus on two power-operating points, namely 0.2 and 1.0 pu active power. At these points, we evaluate the torque ripple, losses, inductance parameters and flux-linkage components for both generators. The performance and parameter results are given in Table IV.

The percentage torque ripple $\Delta\tau$ in Table IV is calculated as the peak-to-peak torque difference as a percentage of the rated torque of the generator. The quality of the actual torque of the generators is shown by the waveforms in Fig. 7. This shows that the hybrid-excited generator has a slightly higher torque ripple; however, the generated torque quality is very much the same as that of the PM generator.

The core losses of the hybrid-excited generator are shown in Table IV to be very much the same as those of the PM generator. This shows that the wound-rotor part of the hybrid-excited generator does not increase the core losses. This is in agreement with the findings of [14] and [15] for non-overlap stator windings with wound-pole rotors, where core losses are shown not to be a particular problem.

TABLE IV
PERFORMANCE RESULTS OF PM- AND HYBRID-EXCITED GENERATORS

Type →	PM		Hybrid	
P(pu)	0.2	1.0	0.2	1.0
Q(pu)	0.08	-0.17	0.08	-0.17
T (pu)	0.2	1.0	0.2	1.0
$\Delta\tau$ (%)	6.36	6.5	6.6	7.4
P_{core} (W)	367	382	340	393
P_{cus} (W)	26.1	569	26.2	564
P_{cuf} (W)	0	0	211	241
X_d (pu)	0.204	0.203	0.36	0.36
X_q (pu)	0.205	0.204	0.32	0.32
X_{dq} (pu)	0.0002	0.0007	0.0004	0.0014
λ_{df} (mWb-t)	0	0	241	257
λ_{qf} (mWb-t)	0	0	0.294	0.348
λ_{dm} (mWb-t)	1073	1071	851	852
λ_{qm} (mWb-t)	1.89	7.65	1.78	8.947
Efficiency (%)	88.4	94.5	85.2	92.8

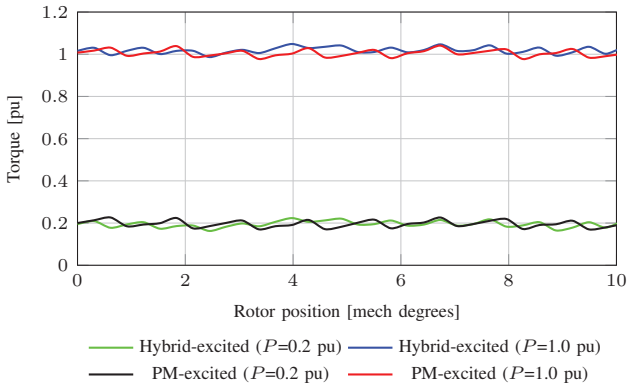

Fig. 7. Torque versus rotor position with load as a parameter for the PM- and hybrid-excited generators.

Table IV shows that the hybrid-excited generator's dq reactances are on average a factor of 1.7 times larger than those of the PM generator's. This is due to the added rotor field winding of the hybrid-excited generator. It is shown that the cross-coupling reactance X_{dq} can be ignored in the analysis of both machines. The important result here is the relatively low per unit synchronous reactance of 0.34 pu of the hybrid-excited generator, which fits well with grid connection.

The flux linkages in Table IV show that the d-axis field and PM-flux linkages of the hybrid-excited generator sum up quite closely to those of the PM generator; this is expected due to the operating voltages being the same. Moreover, it is shown that the q-axis field and PM-flux linkages of both machines can be ignored in the analysis.

The efficiency of the PM generator is shown in Table IV to be higher than that of the hybrid-excited generator. This is due to the additional field-winding copper loss component in the hybrid-excited generator, which is not present in the PM generator.

B. Performance of Grid-tie Hybrid-Excited Generator

In this section, we focus on the performance of the proposed hybrid-excited generator in Fig. 3 in terms of grid-tie requirements. An example of a grid-code power requirement

for renewable energy grid-connected systems is shown in Fig. 8. To evaluate the performance of the grid-tie hybrid-excited generator against the power requirement of Fig. 8, its performance is determined according to Section VI at the red operating dots in Fig. 8 at 0.2 pu and 1.0 pu active powers. The results are shown in Figs. 9 to 13.

The stator copper losses, field copper losses and core losses of the hybrid-excited generator are shown in Fig. 9, and its efficiency in Fig. 10, both versus per unit reactive power. The core losses are the total core losses of the stator and the rotor; we found that the rotor core losses are almost negligibly low. From Fig. 10 it can be seen that the generator's efficiency is at its highest when it is absorbing reactive power, $Q = -0.33$ pu. This is because the field current, and hence the field copper losses, required to achieve this operating power is at a relative minimum. Furthermore, it can be seen that the generator's efficiency at 0.2 pu power decreases sharply as the reactive power increases. This is because the rotor field copper losses increase significantly at these operating conditions as shown in Fig. 9.

The hybrid-excited generator's per unit reactances are shown in Fig. 11. It can be seen that the generator's respective d- and q-axis reactances are constant for varying values of consuming and supplying reactive power. This is because of the constant grid and terminal voltage of the generator, which results in a constant net flux, which keeps the saturation level in the generator constant versus loading. Additionally, it can be seen that the cross-coupling reactance X_{dq} is negligible.

Finally, the induced voltages due to the PM and the field-windings of the hybrid-excited generator are shown in Figs. 12 and 13. These voltages are calculated from (27) as

$$E_{dmf} = E_{df} + E_{dm} = \omega L_{df} I_f + \omega \lambda_{dm} \quad (28)$$

$$E_{qmf} = E_{qf} + E_{qm} = \omega L_{qf} I_f + \omega \lambda_{qm}. \quad (29)$$

Fig. 12 shows that the q-axis-induced voltage E_{qmf} produced by the field-windings and PMs can be considered negligible. Fig. 13 shows the respective field (E_{df}) and PM (E_{dm}) induced voltages, the sum of which produces the E_{dmf} curve shown in Fig. 12. Fig. 13 also shows the field current I_f versus reactive power. It can be seen that a $\pm 20\%$ (E_{df}) voltage is obtained with the change in field current I_f. Both

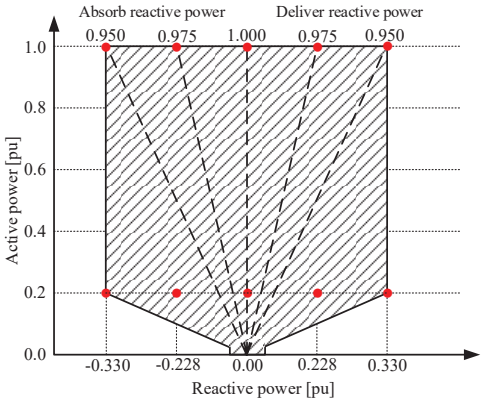

Fig. 8. Example of a grid-connected power versus reactive power requirement.

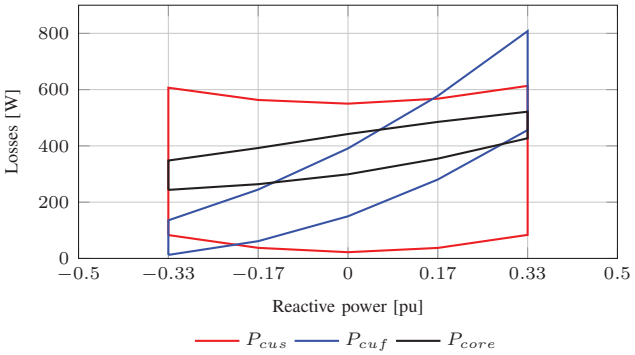

Fig. 9. Generator stator winding (P_{cus}), field winding (P_{cuf}) and core losses (P_{core}) versus reactive power. The bottom curve is for P^* = 0.2 pu and the upper curve is for P^* = 1.0 pu.

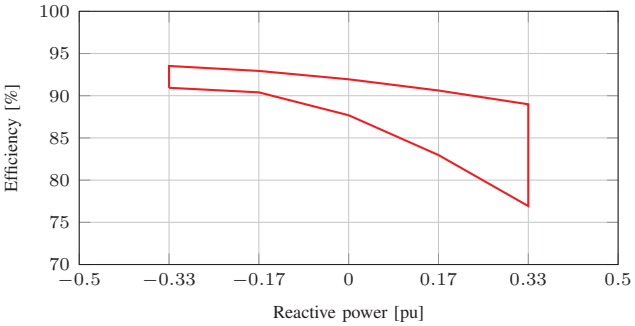

Fig. 10. Generator efficiency versus reactive power. The bottom curve is for P^* = 0.2 pu and the upper curve is for P^* = 1.0 pu.

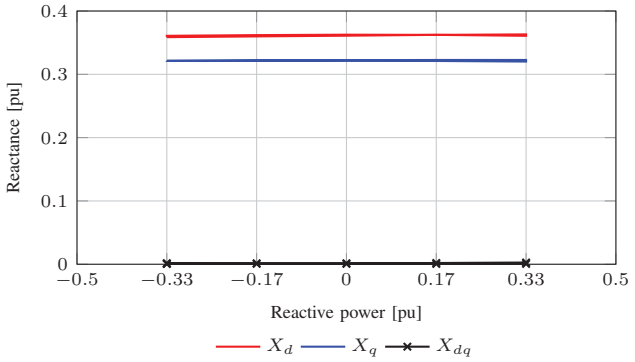

Fig. 11. Per unit reactance X_d (red curve), X_q (blue curve) and X_{dq} (black curve) versus reactive power for P^* = 0.2 pu and for P^* = 1.0 pu.

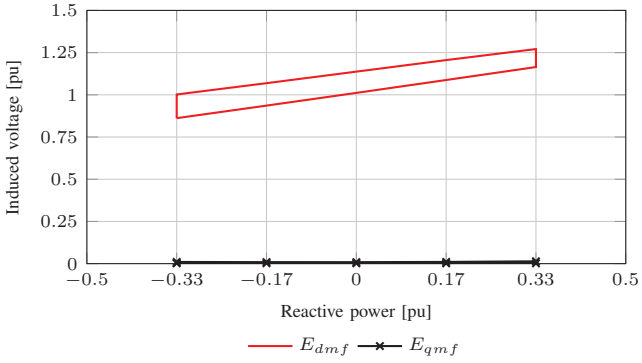

Fig. 12. Generator per unit induced voltage E_{dmf} (red curve) and E_{qmf} (black curve) versus reactive power. The bottom curves are for P^* = 0.2 pu and the upper curves for P^* = 1.0 pu.

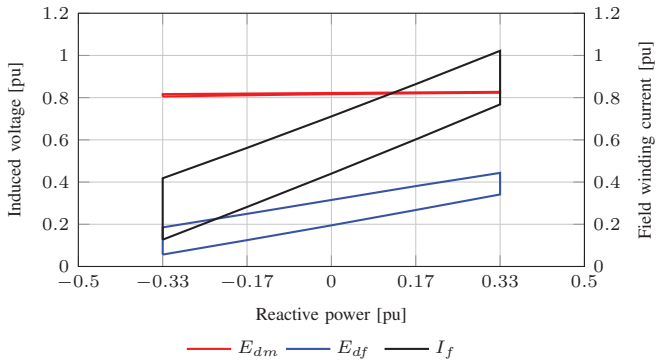

Fig. 13. Generator per unit induced voltage E_{dm} (red curve), E_{df} (blue curve) and I_f (black curve) versus reactive power. The bottom curves are for P^* = 0.2 pu and the upper curves for P^* = 1.0 pu.

E_{df} and I_f never reach zero. The reason for this is the PM induced voltage E_{dm} being slightly too low. Consequently, increasing the PM induced voltage (for example by 0.05 pu) will result in a reduced field current requirement which will improve the efficiency of the hybrid-excited generator.

VIII. Conclusion

In this paper, the feasibility of integrated, parallel hybrid-excited synchronous machines for generator applications are investigated. From the results of the paper, the following conclusions are drawn.

The proposed integrated hybrid-excitation method is shown to be applicable for use in synchronous machines with overlap, but more so with non-overlap stator windings. The method has the disadvantages that it limits the number of parallel circuits of the machine and also limits the possible slot-pole combinations in the case of non-overlap stator windings. These disadvantages, however, become less of a problem as the number of poles of the machine increases.

The proposed method of voltage variation allows the percentage voltage variation to vary from $\pm 10\%$ to a maximum of $\pm 33\%$ by changing the ratio of the number of wound-field poles to the number of magnet poles. This voltage variation fits perfectly with what is required for fixed-frequency, fixed-voltage generators. The FE results obtained from the investigated machine show an almost perfect linear variation of the line voltage versus field current. This proves the purely parallel, independent action of the wound-field and magnet flux excitations of the proposed hybrid-excited rotor.

Accurate FE analysis show that the proposed grid-tie hybrid-excited generator adheres perfectly to the reactive power grid-code requirements by being able to consume/supply up to 0.33 pu reactive power. The frozen permeability FE analysis further reveals that the cross-coupling reactances and q-axis induced voltages can be ignored in the dq analysis of the proposed hybrid-excited generator.

The core losses and torque ripple of the hybrid-excited generator are shown to be similar to those of an equivalent PM generator. Its efficiency, however, is less than that of the PM generator due to the additional rotor field-winding copper losses.

The proposed hybrid-excited generator's dq reactance is found to be a factor of 1.7 larger than that of the equivalent surface-mount PM generator. However, in spite of the added rotor field-winding part, a significant result is that the synchronous reactance of the grid-tie hybrid-excited generator is still relative low, at 0.34 pu. This will ensure excellent grid strength with grid fault support of close to 3.0 pu current.

References

[1] D. Fodorean, A. Djerdir, I.-A. Viorel, and A. Miraoui, "A double excited synchronous machine for direct drive application: design and prototype tests," IEEE Transactions on Energy Conversion, vol. 22, no. 3, pp. 656–665, 2007.

[2] K. Kamiev, A. Parviainen, and J. Pyrhönen, "Hybrid excitation synchronous generators for small hydropower plants," IEEE International Conference on Electrical Machines (ICEM), Lausanne (Switzerland), Sept. 2016

[3] G. Henneberger, J. R. Hadji-Minaglou, and R. C. Ciorba, "Design and test of permanent magnet synchronous motor with auxiliary excitation winding for electric vehicle application," in Proc. European Power Electronics Chapter Symposium, Lausanne (Switzerland), pp. 645–649, Oct. 1994.

[4] F. Leonardi, T. Matsuo, Y. Li, T. A. Lipo, and P. J. McCleer, "Design considerations and test results for a doubly salient PM motor with flux control," in Conf. Record IEEE IAS Annual Meeting, vol. 1, pp. 458–463, 1996.

[5] X. Luo and T. A. Lipo, "A synchronous/permanent magnet hybrid AC machine," IEEE Transactions on Energy Conversion, vol. 15, no. 2, pp 203–210, June 2000.

[6] Y. Amara, L. Vido, M. Gabsi, E. Hoang, A. H. B. Ahmed, and M. Lecrivain, "Hybrid excitation synchronous machines: Energy-efficient solution for vehicles propulsion," IEEE Transactions on Vehicular Technology, vol. 58, no. 5, pp. 2137–2149, 2009.

[7] K. Kamiev, J. Nerg, J. Pyrhönen, and V. Zaboin, "Hybrid excitation synchronous generators for island operation," in the XIX International Conference on Electrical Machines (ICEM), Rome (Italy), 2010.

[8] K. Yamazaki, K. Nishioka, K. Shima, T. Fukami and K. Shirai, "Estimation of assist effects by additional permanent magnets in salient-pole synchronous generators," IEEE Trans. on Industrial Electronics, vol. 59, no. 6, pp. 2515-2523, 2012.

[9] L. L. Amuhaya and M. J. Kamper, "Design and optimisation of grid compliant variable-flux PM synchronous generator for wind turbine applications," IEEE Energy Conversion Congress and Exposition (ECCE), Montreal (Canada), pp. 829–836, Sept. 2015.

[10] M. Ployard, F. Gillon, A. Ammar, D. Laloy, and L. Vido, "Hybrid excitation topologies of synchronous generator for direct drive wind turbine," in IEEE Energy Conversion Congress and Exposition (ECCE), Milwaukee, WI (USA), September 2016.

[11] W. Chai, B. Kwon and T.A. Lipo, "Rotor shape optimization for improving torque performance of PM-assisted wound field synchronous machines," IEEE International Magnetics Conference (INTERMAG), Singapore, April 23-27, 2018

[12] Sami Hlioui, Yacine Amara, Emmanuel Hoang, Michel Lecrivain, Mohamed Gabsi, "Overview of hybrid excitation synchronous machines technology, ICEESA, 2013

[13] D. Ockhuis, M. J. Kamper and A. T. Loubser, "Impedance Matching of Direct Grid-Connected Renewable Energy Synchronous Generators," 2020 International SAUPEC/RobMech/PRASA Conference, Cape Town, South Africa, 2020.

[14] J. Jürgens, A. Brune and B. Ponick, "Electromagnetic design and analysis of a salient-pole synchronous machine with tooth-coil windings for use as a wheel hub motor in an electric vehicle", 2014 International Conference on Electrical Machines (ICEM), pp. 744-750, 2-5 Sept. 2014.

[15] K.S. Garner and M.J. Kamper, "Reducing MMF harmonics and core loss effect of non-overlap winding wound rotor synchronous machine (WRSM)", IEEE Energy Conversion Congress and Expo (ECCE 2017), Cincinnati, OH (USA), pp. 1850-1856, 1-5 October, 2017.